A new benchmark T8-9 brown dwarf and a couple of new mid-T dwarfs from the UKIDSS DR5+ LAS^*

B. Goldman¹†, S. Marsat¹, T. Henning¹, C. Clemens², and J. Greiner²

Max Planck Institute for Astronomy, Koenigstuhl 17, D-69117 Heidelberg, Germany

- ² Max Planck Institute for extraterrestrial Physics, Giessenbachstraße, D-85748 Garching, Germany

ABSTRACT

Benchmark brown dwarfs are those objects for which fiducial constraints are available, including effective temperature, parallax, age, metallicity. We searched for new cool brown dwarfs in 186 sq.deg of the new area covered by the data release DR5+ of the UKIDSS Large Area Survey. Follow-up optical and near-infrared broad-band photometry, and methane imaging of four promising candidates, revealed three objects with distinct methane absorption, typical of mid- to late-T dwarfs, and one possibly T4 dwarf. The latest-type object, classified as T8-9, shares its large proper motion with Ross 458 (BD+13°2618), an active M0.5 binary which is 102" away, forming a hierarchical low-mass star+brown dwarf system. Ross 458C has an absolute J-band magnitude of 16.4, and seems overluminous, particularly in the K band, compared to similar field brown dwarfs. We estimate the age of the system to be less than 1 Gyr, and its mass to be as low as 14 Jupiter masses for the age of 1 Gyr. At 11.4 pc, this new late T benchmark dwarf is a promising target to constrain the evolutionary and atmospheric models of very low-mass brown dwarfs. We present proper motion measurements for our targets and for 13 known brown dwarfs. Two brown dwarfs have velocities typical of the thick disk and may be old brown dwarfs.

Key words: stars: low-mass, brown dwarfs – binaries: general – stars: individual: Ross 458C.

INTRODUCTION

Cool brown dwarfs with effective temperatures lower than 1800 K are characterized by complicated and diverse atmospheric processes that profoundly affect their emerging spectral energy distribution (e.g. Saumon & Marley 2008). Atmospheric models have been much improved over the last decade (Allard et al. 2001; Tsuji 2005; Burrows et al. 2006; Saumon & Marley 2008; Helling et al. 2008). Dynamical processes are investigated through observations (Leggett et al. 2009) and simulations (Helling et al. 2008). Increasing the searched volume may reveal peculiar objects in terms of colours, metallicity and age (e.g. Burgasser 2004; Kirkpatrick et al. 2008) and lower effective temperatures.

A valuable sub-class of brown dwarfs are those for which we can obtain more information than is usually the case for

* Based on observations collected at the German-Spanish Astronomical Center, Calar Alto, jointly operated by the Max-Planck-Institut für Astronomie Heidelberg and the Instituto de Astrofísica de Andaluca (CSIC); and on observations made with ESO/MPG Telescope at the La Silla Observatory under programme ID 081.A-9012 and 081.A-9014.

† E-mail: goldman@mpia.de

isolated brown dwarfs. As brown dwarfs cool with age, it is difficult to disentangle the effects of an higher mass and an younger age; gravity measurements are difficult to obtain for those faint objects, and high-spectral resolution modeling is complex. Objects associated with a cluster, or a brighter companion, especially when they are close enough to allow high signal-to-noise spectroscopy, may be used as benchmark brown dwarfs (Pinfield et al. 2006; Burningham et al. 2009).

There are nine such systems including a T-type companion. Leggett et al. (2002), for instance, have studied the first two field L- and T-type brown dwarfs companions to main sequence stars, the T dwarf Gl 229B (Nakajima et al. 1995) and the L dwarf LHS 102B (Goldman et al. 1999), to derive the substellar parameters of those objects and confirm the evolutionary models. Very recently, Faherty et al. (2010) presented a M3+T6.5 binary, G 204-39 and SDSS J1758+4633, with an age of 0.5-1.5 Gyr, as well as one of the weakliest bound system, a G5+L4 binary with a 25,000-AU projected separation, G 200-28 and SDSS J1416+5006. Finally, Burningham et al. (2009) found a M4+T8.5 system in the UKIDSS LAS DR 4, Wolf 940 AB, whose primary's low activity level indicates an age of 3.5–6 Gyr.

Recent surveys, such as 2MASS, DENIS or SDSS have brought a wealth of new neighbours of always cooler temperatures (Delfosse et al. 1999; Kirkpatrick et al. 2000; Leggett et al. 2000). The UKIDSS set of surveys, with a gain in volume of two dozens, push this research forward (Lawrence et al. 2007). In its high-galactic latitude, shallow component, the Large Area Survey (LAS), more than 30 new T dwarfs have been discovered, including the coolest compact objects outside the Solar system (Lodieu et al. 2007; Warren et al. 2007; Chiu et al. 2008; Pinfield et al. 2008; Burningham et al. 2008), along with the CFHT-LS survey (Delorme et al. 2008).

We have searched the area newly covered by the data release DR5+ of April 2009 of UKIDSS-LAS for new cool brown dwarfs of spectral type T. Using a simple colourcut selection, we selected targets for photometric follow-up. Here, we report on the discovery of a new benchmark T8-9 brown dwarf located at 11 pc, and of 3-4 new mid-T brown dwarfs.

To obtain a preliminary spectral classification, we rely on methane imaging. Spectra of mid-T dwarfs and latertype brown dwarfs are known to exhibit strong methane (and water) absorption in the red half of the H band. This feature distinguishes them from all celestial bodies warmer than 1400 K. Relatively short exposure times in the 0.1- μ m-wide filters offer a robust confirmation and a preliminary spectral classification of brown dwarf candidates (see Appendix A). This method has been successfully used by Tinney et al. (2005) to confirm candidates found in 2MASS and Lodieu et al. (2009), in the UKIDSS Deep Extragalactic Survey.

We establish the companionship of ULAS J130041+122114 with Ross 458 (BD+13°2618, GJ 494, HIP 63510) in Section 3, and refer to it as Ross 458C for simplicity. Ross (1926) discovered the proper motion of Ross 458. His work allows us to establish the companionship with our target, and we therefore choose this name among all the possible names of Ross 458.

We first describe our selection criteria and follow-up observations and data reduction. In Section 3 we discuss the companionship of Ross 458C with Ross 458AB. Finally, in Section 4 we study the properties of the new brown dwarfs and brown dwarf candidates. The calibration of the methane filter set of Omega 2000 is detailed in the Appendix A.

2 CANDIDATE SELECTION AND FOLLOW-UP OBSERVATIONS

2.1 Mining the UKIDSS DR5+ of the LAS

In this subsection we discuss how we selected the four objects for follow-up observations. We do not intend in this article to search for cool brown dwarfs systematically and we refer to a later article (and a larger sample) for a proper detection selection and efficiency estimate.

Known cool brown dwarfs (mid-T type and later) are red in their optical and Y-J colour and blue in their near-IR colours. The former is primarily due to the absorption by alkali elements such as Na I and K I, while the latter is due to the absorption by water and methane. This behaviour is predicted by models (Burrows et al. 2003), and confirmed by observations of 2MASS and SDSS brown dwarfs (Hewett et al. 2006), as well as recent UKIDSS discoveries (Warren et al. 2007; Lodieu et al. 2007; Pinfield et al.

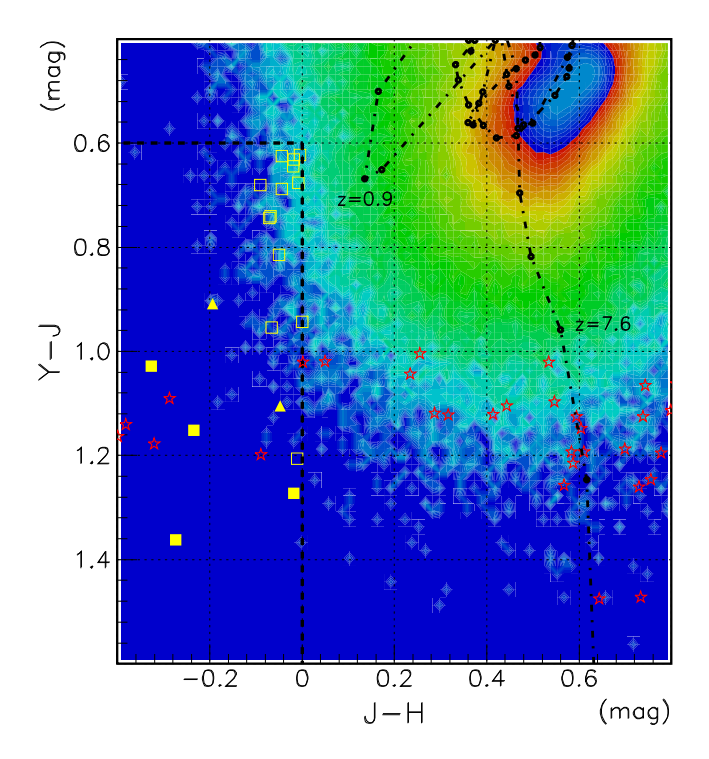


Figure 1. Y-J vs. J-H colour-colour diagramme for UKIDSS DR5+. The selection cuts are indicated by the dashed lines. The targets described in this paper are shown as full squares, while the empty squares indicate objects with an SDSS cross-match. The two triangles indicate good targets for which we could not obtain methane imaging data. The grey shades scale as the logarithm of the stellar density, with black for the highest density of the stellar locus, selected over the whole area of DR5+ with the same quality cuts as our candidate sample. Empty stars show known brown dwarfs; the dash-dotted line shows the predicted quasar locus, with redshift steps of 0.1 (Hewett et al. 2006).

2008). Burningham et al. (2008) searched for Y-J>0.5 and J-H<0.1 objects and the finding closest to these colour cuts (in a sample of three) has UKIDSS colours of $Y-J=0.60\pm0.07$ and $J-H=-0.25\pm0.03$. Fig. 1 summarizes these results.

We search the UKIDSS DR5+ data release of the LAS for objects with YJH detections and photometric errors smaller than 30 mmag; YJ ppErrBits quality flags smaller than 256; a J-band magnitude between 15.0 and 20.0 mag; a probability to be stellar larger than 0.6 and a class star parameter mergedClass of -1. The objects should fulfill the following colour constraints (using 2"-radius aperture photometry): Y-J>0.6 mag, J-H<0.0 mag and either H-K<0.25 mag if the object is detected in the K band, or $H-{\rm depth}_K<0.25$ where ${\rm depth}_K$ is the limiting magnitude (3σ) in a 2"-radius aperture. In order to avoid duplicating observations, we perform the same search on the DR4+ LAS data release and exclude from the DR5+ results the objects found identical in the DR4+ results.

For the purpose of our follow-up GROND programme (with scheduled times at the beginning of the night, see subsection 2.2), we requested a right ascension between 7 and 14 hours. This returns 19 candidates. Among those, 13 objects, which have -0.1 < J - H < 0.0, are matched within 3" with a SDSS griz source and have spectral types ear-

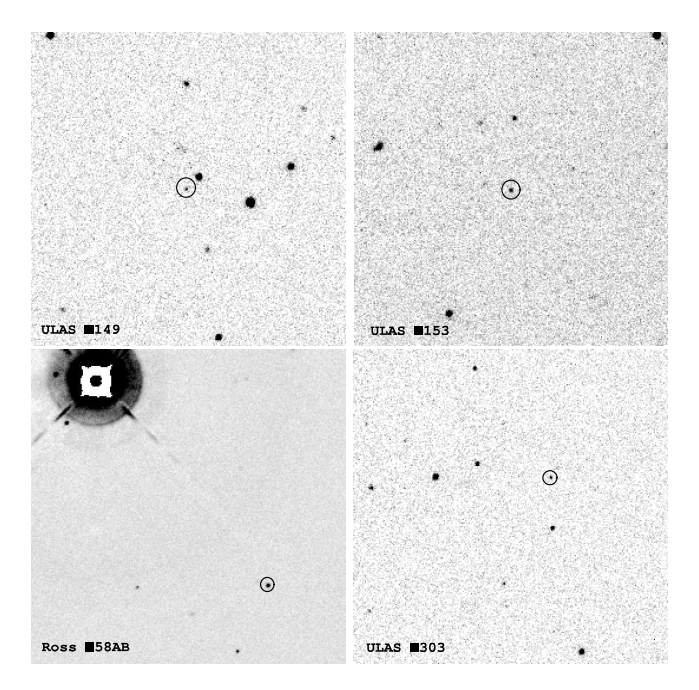


Figure 2. Finding charts based on Omega 2000 methane off images. The fields are 2 arcmin on each side; North is up and East is left.

lier than M6 (West et al. 2005). Six objects remain and we obtained follow-up data for the four bluest objects, with J-H<-0.05, leaving out the two objects with -0.05 < J-H < 0. The finding charts are given in Fig. 2. We did not perform astrometric cuts.

We perform a rough estimate of the area searched for this work: we count the number of distinct $(6.8')^2$ footprints (one quarter of a WFCam chip) with at least one stellar-type object with YJHK detections and quality parameters similar to our T dwarf selection (in terms of photometric errors and quality flags). We subtract the similar number obtained for DR4+ (10881 footprints) from the DR5+ number (14630) and find an area of 186 sq.deg. Because the LAS footprint is mostly contiguous, the (reasonable) choice of a different footprint size and/or origin changes the result by no more than 5%.

2.2 GROND follow-up photometry

In April 2009 we obtained broad-band g'r'i'z'JHK imaging data of the brown dwarf candidates, using GROND on the ESO/MPG 2.2m telescope located in La Silla. GROND is a simultaneous imager which uses six dichroics to split the beam into the seven channels (Greiner et al. 2007, 2008). The GROND photometric system is close to SDSS's in the optical and to 2MASS's in the near-infrared. The main difference is in the i filter: as the SDSS riz filters overlap at their $\sim 70\%$ transmission values, the GROND i is narrower than the SDSS i filter. However, the central wavelengths are very close. The colour transformations into the SDSS AB and 2MASS Vega systems of Greiner et al. (2008) lists negligible colour corrections, except for the J band. Because we do not have enough observations of T-type brown dwarfs to improve the photometric calibration for that spectral class,

Table 1. Observing logs from GROND and Omega 2000

Instrument	GRO	OND	Omega	a 2000
Target	Date^1	$Seeing^2$	Date^1	Seeing
ULAS J1149-0143	April 29	1.5"	May 8	1.2"
ULAS J1153 -0147	April 22	1.2"	May 12	1.1''
Ross 458C	April 22	1.4"	May 12	1.0''
ULAS J $1303+1346$	April 30	1.9"	May 12	0.9''

 $^{^{1}}$ Year 2009. 2 As measured on the *J*-band images.

we report here the photometry in the GROND system, with no colour correction applied.

We observed all targets with the 20m4td observation block, with slow read-out mode, four dither positions, 20 min total integration time in JHK and 24.6 min in g'r'i'z'. We describe the observations of the four objects reported in this article in Table 1.

We reduced the data using the GROND pipeline, which is based on the Pyraf/IRAF libraries (Greiner et al. 2008). The pipeline corrects the individual images for bias, dark and flat-field. It then corrects for geometrical distortions, sky-subtracts the near-IR images, and shifts and coadds the dithered images. The source catalogues, positions and aperture photometry are extracted using SExtractor (Bertin & Arnouts 1996). Finally, the astrometry is corrected for rotation, pixel scale and translation using the SDSS and 2MASS catalogues as reference, and the photometric zero points can be determined using the same catalogues.

We actually re-determine the zero points, using a few dozen stars observed by the SDSS and UKIDSS. We previously transform the SDSS photometry into the GROND system using the colour transformations of Greiner et al. (2008), and the UKIDSS photometry into the 2MASS system using the transformations of Hewett et al. (2006). The typical precision is 5%, to be added to the SDSS (1–2%) and UKIDSS (4%) calibration accuracy. The GROND photometry is listed in Table 3. We do not include the calibration errors in the photometric errors reported in that table. For non-detections (gri bands), we report the 10- σ limit, calculated as the average magnitude of objects with 0.1-mag errors

We refine the image registration of the GROND co-added images using scamp (Bertin 2006). We use as reference catalogue the UKIDSS positions measured in the band of the closest central wavelength. Bright objects (SNR>30, a few dozens) are used to derive a preliminary transformation, which is refined with all objects with SNR>3 (one hundred). We use second-order polynomial transformations. The typical positional dispersion in each direction is 30–70 mas for the bright star sample, depending on the filters and fields. We add quadratically this dispersion to the photo-noise centring error reported by SExtractor.

2.3 Omega2000 methane imaging

The methane imaging is an efficient method to obtain confirmation and preliminary spectral typing of faint T dwarf candidates using medium-size telescopes. Some extragalactic contaminants may mimic T-dwarf methane colours, if

4 B. Goldman et al.

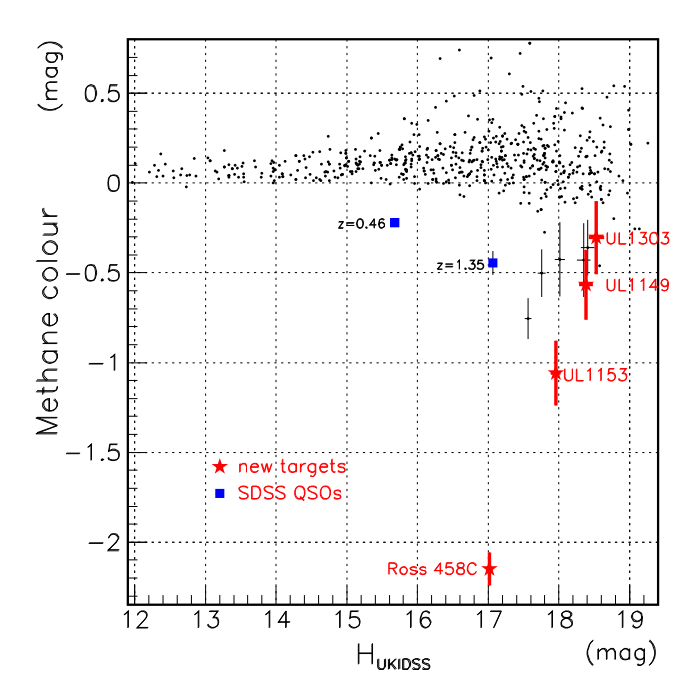


Figure 3. Methane colour for our new objects (stars, with statistical error bars), and the field stars in their fields. We signal two known quasars, LBQS 1146-0128 with z=0.46 and SDSS J130324.21+134045.0 with z=1.35. We also indicate the error bars of objects with large, suspicious methane colour. Most are artefacts.

their spectrum shows a strong emission line which may fall into the methane off filter transmission for certain redshifts. Quasars have strong H α emission (among other lines) and for redshifts z=1.30–1.48 have AB methane colours of -0.27 to -0.73 (at z=1.41). We have indeed detected two known and one new quasars over 1 sq.deg. (see Section 2.3). However, quasars at those redshifts are easily detected in the optical and show optical colours clearly different from those of T dwarfs.

As the GROND photometry and astrometry supported the brown dwarf hypothesis for these four targets, we obtained DDT observations in the H-band methane on and off medium-band filters of the Omega 2000 near-infrared wide-field imager on the Calar Alto 3.5-m telescope (Bailer-Jones et al. 2000).

In May 2009, we obtained 6-min total-integration time observations in the methane off filter and 25-min integrations in the methane on filters. The observations are described in Table 1. The integrations were split in 1-min coadded images of six 10-sec integrations. Between each coadded image we dithered the telescope to allow for sky and bias subtraction.

The observing set-up and photometric data reduction is similar to those performed to calibrate the Omega 2000 methane filter set. We refer the reader to the appendix A for details regarding the method and the data analysis. The astrometry was derived in a similar way as for the GROND observations, using SExtractor and scamp, and we refer the reader to Section 2.2. We find that the dispersion of positions relative to the reference catalogue is minimised for a first-degree polynomial transformation.

We report the science targets' methane colour and the

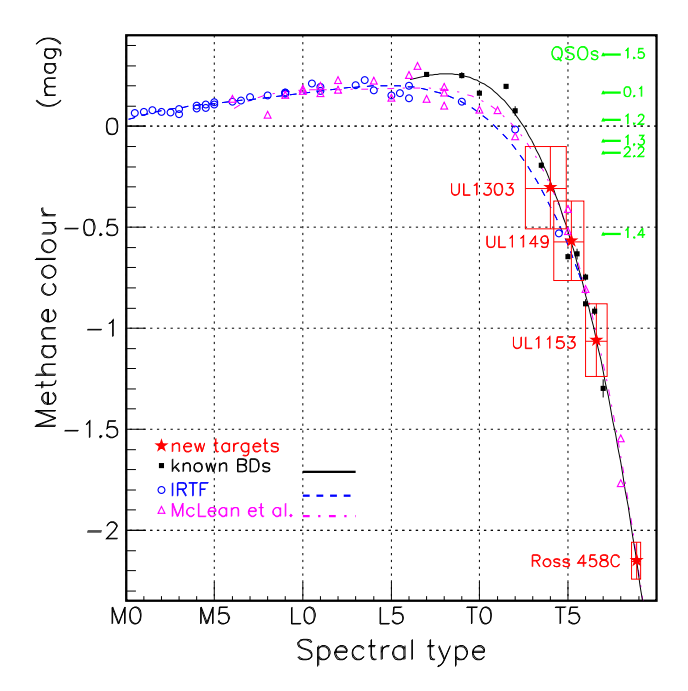


Figure 4. Methane colour for our new objects (stars, with statistical error boxes), the reference brown dwarfs (squares, with statistical error bars), and synthetic photometry using the McLean et al. (2003) and IRTF spectral libraries (triangles and circles respectively). We superimpose the polynomial fits for the observed indices (third-degree polynome; in black solid line) and synthetised indices (fourth-degree polynomes; in blue dashed line: IRTF, in magenta dash-dotted line: McLean et al.). See Appendix A for details. We indicate some methane colours of quasars with redshifts between 0 and 4.

spectral type derived from it, along with 1- σ error bars, in Table 3. They are illustrated in Fig. 3 and 4. The statistical error includes only the photo-noise on the targets' methane colour measurements, while the systematic errors indicate the calibration errors (see Subsection A4).

We derive the photometric distances based on the spectral type and the J, H and K magnitudes (see Table 3 and subsection 4.1.2).

2.4 Proper motions

We use the astrometry derived from the UKIDSS DR5+, GROND and Omega 2000 data to measure the proper motion of our candidates. The UKIDSS H and K images were obtained in 2007 for Ross 458C or in 2008 for the rest of the sample, the Y and J images in 2008, and the GROND and Omega 2000 images in 2009, resulting in a 1- or 2-year (Ross 458C) baseline.

We perform the image registration of the Omega 2000 and GROND images using the UKIDSS DR5+ catalogue as the astrometric reference, using the closest filter, in terms of central wavelength.

We assign an accuracy of 20 mas for each UKIDSS position. We confirm this rough estimate, originally based on the UKIDSS position residuals, by using the J-band second-epoch observations over 42-sq.deg., released in DR6+. The relative position root-mean-square is 33 mas along the right ascension, and 35 mas along the declination, for stars with

15 < J < 19 and a signal-to-noise ratio larger than 20. With a time baseline of 2–3 years, some of the dispersion is due to the real proper motions, and a Besançon simulation of those stars estimates this contribution to a small 5 mas/yr (Robin et al. 2003). Assuming Gaussian, independent noise on each epoch position, the single-frame accuracy in each direction is about 22 mas for this sample.

The GROND and Omega 2000 errors include the photonoise accuracy and the systematics due to the registration process. The proper motion fit assumes that all errors are independent. The systematics introduced by the reference catalogue errors also propagate to all GROND and Omega 2000 measurements.

We report all the measurements for Ross 458C in Table 2, and the proper motions of all targets in the same table. We give $\mu_{\alpha} = \frac{d\alpha}{dt}$ rather than the projection of the proper motion along α . We similarly derived proper motions of the brown dwarfs used to derive the calibration of the Omega2000 methane filter set, and those are presented in section A5 and Table A2.

3 COMPANIONSHIP TO ROSS 458

Several independent measurements of the proper motion of Ross 458AB (also DT Vir, BD+13°2618) are available in the literature. We quote a selection in Table 2. Hereafter we use the Hipparcos measurement for simplicity; in most cases the conclusions are identical for all values.

The proper motions of Ross 458AB and Ross 458C agree within 0.5σ in both directions. Ross 458AB is detected in the Luyten Half-Second catalogue (LHS), with a proper motion of 0.714''/yr (Luyten 1979), and is bright enough to be included in the Hipparcos catalogue (Perryman et al. 1997). There are 2120 stars with proper motions larger than 0.6''/yr in the LHS catalogue, or one every 20 sq.deg. Among those there are 639 objects with an Hipparcos parallax measurement, and 308 have a distance between 5 and 20 pc, compatible with the photometric parallax of Ross 458C. The number of such objects over a 5-arcmin-radius disk is 2.10^{-4} .

Ignoring the distance constraints, but considering the small proper motion difference: there are 443 stars with proper motion within 1σ of Ross 458C's proper motion in the LHS catalogue (Luyten 1979). (At the brightness of Ross 458AB, the LHS catalogue is close to complete.) In addition, the proper motion direction of Ross 458C is known to $\pm 2 \deg (1\sigma)$, so that we expect 5 stars over the sky to share its proper motion within the uncertainties, or 3.10^{-6} over the 5-'-radius disk area. Searching for stars with proper motions within 5σ (to increase the statistics) of Ross 458C's in Salim & Gould (2003), which covers three quarters of the sky, returns 143 stars, or 7.6 stars for a 1σ interval over the whole sky.

Fig. 5 illustrates the rare match of the proper motions of Ross 458AB and our target. We show the proper motions we measure for all field objects around Ross 458 and ULAS J1153, as well as the high proper motions ($\mu > 0.2\,\mathrm{''/yr}$) from van Leeuwen (2007) and Roeser et al. (2008) (other proper motion catalogues give similar results) within 1 deg of the targets.

Either way, the probability for Ross 458AB and Ross 458C to be chance neighbours is negligible.

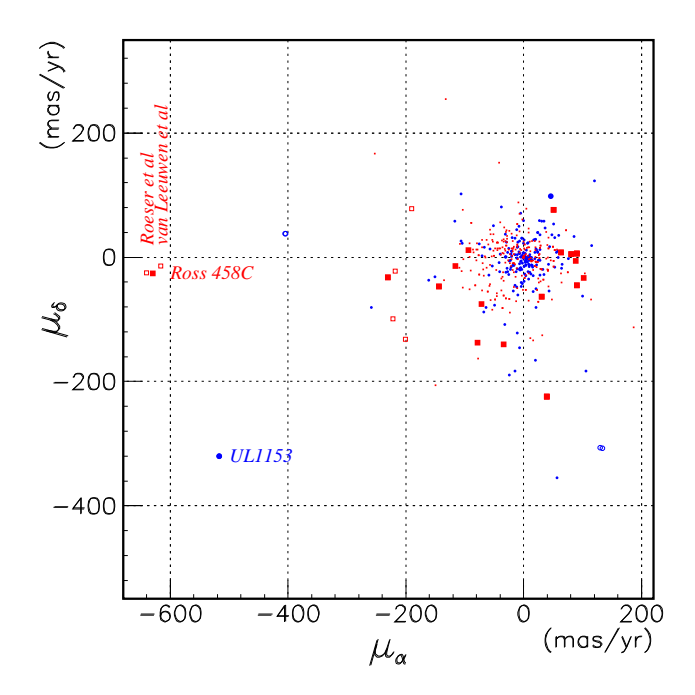


Figure 5. Measured proper motion vectors of the 15-arcmin field objects around Ross 458 (squares) and ULAS J1153 (circles); large symbols show significant proper motions at the $3-\sigma$ level. Open symbols show catalogued stars with proper motions larger than 0.2''/yr, within 1 deg of the targets (from van Leeuwen (2007) and Roeser et al. (2008), see text).

4 PROPERTIES OF THE NEW BROWN DWARFS

4.1 Ross 458C

4.1.1 Properties of Ross 458AB

Ross 458AB is a binary made of a M7 dwarf orbiting a M0.5 dwarf (although early references report M2, or even M3), with a 14.5-yr period (Heintz 1994). The separation was 0.475" in February 2000, or 5.4 AU (Beuzit et al. 2004). However, the latter authors point out an inconsistency between their measurements and the results of Heintz (1994).

Ross 458A is very active, as indicated by its H α emission strength and variability (see Table 4). West et al. (2008) estimate an age of 400 ± 400 Myr for M1 active dwarfs. Its rotational velocity of $10 \, \mathrm{km/s}$ means it is not tidally-locked, also implying an age smaller than $\sim 1 \, \mathrm{Gyr}$.

The space velocity presented by Montes et al. (2001) makes it a possible member of the Hyades supercluster, which has a space velocity of $(U,V,W)=(-40,-17,-3)\,\mathrm{km/s}$ (Zuckerman et al. 2004). Considering other published proper motions does not change this conclusion. The age of the Hyades is estimated at $(648\pm45)\,\mathrm{Myr}$ (DeGennaro et al. 2009). However the members of its moving group show a dispersion in age $(0.4-2\,\mathrm{Gyr})$ and metallicity. Possibly the common motion should be attributed to tidal effects of the massive rotating bar, rather than a common birthplace. The metallicity of the cluster of $[\mathrm{Fe/H}] = +0.14$ is compatible with the solar metallicity estimate of Alonso et al. (1996). We note, however, that Hawley et al. (1997) report a radial velocity of $-43.4\,\mathrm{km/s}$, leading to

6 B. Goldman et al.

Table 2. Astrometric data on Ross 458AB, of our targets and of the calibration brown dwarfs, as well as the photometric distance and tangential velocity.

Name	Ref.	MJD or Epoch	RA (J2000) hms	DEC (J2000) dms	$\mu_{\alpha} \ (\mathrm{mas/yr})$	μ_{δ} (mas/yr)	dist. pc	$v_{\perp} \ m km/s$
Ross 458AB	(1)	2000.0	13:00:46.582	+12:22:32.604	-618.8 ± 1.8	-16.6 ± 1.3	11.4 ± 0.2	33.4 ± 0.6
$(BD+13^{\circ}2618)$	(2)				-636.2	-25.5		
	(3)				-641.2	-23.7		
	(1)	2007.97	13 00 46.245	$+12\ 22\ 32.47$	_	_		
Ross 458C	UKIDSS Y	54572.5	13 00 41.729	+12 21 14.69				
	UKIDSS J	54572.5	$13\ 00\ 41.730$	$+12\ 21\ 14.73$				
	UKIDSS H	54224.5	$13\ 00\ 41.771$	$+12\ 21\ 14.75$				
	UKIDSS K	54224.5	$13\ 00\ 41.771$	$+12\ 21\ 14.75$				
	GROND z	54943.13	$13\ 00\ 41.698$	$+12\ 21\ 14.73$				
	GROND J	54943.13	$13\ 00\ 41.688$	$+12\ 21\ 14.73$				
	GROND H	54943.13	$13\ 00\ 41.696$	$+12\ 21\ 14.73$				
	GROND K	54943.13	$13\ 00\ 41.696$	$+12\ 21\ 14.65$				
	O2000 on	54960.02	$13\ 00\ 41.683$	$+12\ 21\ 14.72$				
	O2000 on	54963.97	$13\ 00\ 41.683$	$+12\ 21\ 14.66$				
	O2000 off	54963.98	$13\ 00\ 41.675$	$+12\ 21\ 14.81$				
	fit	2007.97	$13\ 00\ 41.743$	$+12\ 21\ 14.72$	-629 ± 29	-23 ± 26		
	(1)	2000.0	13 00 42.080	$+12\ 21\ 14.86$	-618.8 ± 1.8	-16.6 ± 1.3		
ULAS J1149-0143	=	2008.28	11 49 25.584	-01 57 08.28	-51 ± 91	+9±85	53	13
ULAS J1153-0147	_	2008.29	$11\ 53\ 38.735$	$-01\ 36\ 25.56$	-517 ± 73	-321 ± 72	29	85
ULAS J1303+1346	_	2008.25	13 03 18.281	$+13\ 56\ 46.32$	$+36\pm76$	-92 ± 76	73	34

⁽¹⁾ Perryman et al. (1997). (2) Zacharias et al. (2003). (3) Ducourant et al. (2006).

Table 3. Photometry of our targets. The UKIDSS YJHK magnitudes are in the WFCam Vega system; GROND iz (or 10- σ limits) are in the GROND AB system; the Omega 2000 methane colour is in the Vega system.

Name	$z_{ m SDSS}$	$Y_{ m UKIDSS}$	$J_{ m UKIDSS}$	$H_{ m UKIDSS}$	$K_{ m UKIDSS}$	spectral type \pm (stat) \pm (sys)
ULAS J1149-0143 ULAS J1153-0147 Ross 458C ULAS J1303+1346	$ 20.24 \pm 0.19$ $-$	19.30 ± 0.07 19.04 ± 0.06 17.72 ± 0.02 19.78 ± 0.08	18.15 ± 0.05 17.68 ± 0.04 16.69 ± 0.01 18.51 ± 0.04	18.38 ± 0.10 17.95 ± 0.07 17.01 ± 0.04 18.53 ± 0.11	18.34 ± 0.20 17.72 ± 0.12 16.90 ± 0.06 18.58 ± 0.18	$T5.2^{+0.9}_{-1.2} \pm 1$ $T6.6 \pm 0.8 \pm 0.3$ $T8.9 \pm 0.3 \pm 0.2$ $T4.0^{+1.3}_{-1.8} \pm 1$
Name	$i'_{ m GROND}$	$z'_{ m GROND}$	J_{GROND}	H_{GROND}	K_{GROND}	
ULAS J1149-0143 ULAS J1153-0147 Ross 458C ULAS J1303+1346	> 23.12 > 23.16 > 21.3 > 22.77	22.40 ± 0.38 21.62 ± 0.27 20.86 ± 0.20 > 22.59	18.40 ± 0.05 17.92 ± 0.05 16.97 ± 0.03 18.84 ± 0.06	18.19 ± 0.06 17.95 ± 0.05 17.02 ± 0.03 19.20 ± 0.10	$ 18.01 \pm 0.10 16.46 \pm 0.05 19.33 \pm 0.20 $	
Name	$z_{ m GROND}$ $-$	$Y = (Y - J)_{\mathrm{U}}$	$_{ m KIDSS}$ $(J-I)$	$H)_{\text{UKIDSS}}$ (H	$-K)_{\text{UKIDSS}}$	CH_4 colour
ULAS J1149-0143 ULAS J1153-0147 Ross 458C ULAS J1303+1346	1.10 ± 0.3 2.63 ± 0.2 3.08 ± 0.1 > 2.81	$+1.36 \pm$	$\begin{array}{ccc} 0.07 & -0.2 \\ 0.03 & -0.3 \end{array}$	$27 \pm 0.08 + 33 \pm 0.04 + 43$	0.04 ± 0.22 0.23 ± 0.14 0.09 ± 0.07 0.05 ± 0.21	-0.57 ± 0.20 -1.06 ± 0.18 -2.15 ± 0.11 -0.30 ± 0.20

 $W=-40\,\mathrm{km/s}$, which would be incompatible with a Hyades moving group membership.

Taking into account these various constraints we estimate the age of Ross 458AB to less than 1 Gyr. We summarise the properties of Ross 458AB in Table 4.

4.1.2 Interpretation

Given the parallax of Ross 458AB, we deduce the absolute magnitudes of Ross 458C to be: $M_J=16.40\pm0.04$ and $M_K=16.61\pm0.06$ in the WFCam system. We convert

the UKIDSS photometry into the 2MASS system using the colour transformations we derived in section B., and place in Fig.6 our target in the absolute magnitude vs. spectral type diagram, along with 21 known brown dwarfs with trigonometric parallax (excluding known close binaries). The spread of magnitudes for a given spectral type is large in the sample, certainly due to variations in the gravity (i.e. mass/age), unresolved binaries, and to a lesser extend metallicity. We nevertheless fit the 2MASS photometry with a second-degree polynomial:

Table 4. Description of Ross 458AB.

Parameter	Component	Value	Unit	Reference
Type	A	M0.5		Hawley et al. (1997)
	В	M7		Beuzit et al. (2004)
Mass	A	0.6	${ m M}_{\odot}$	Leggett (1992)
	В	0.06 – 0.09	${ m M}_{\odot}$	Baraffe et al. (1998)
Age	A	≤ 1	Gyr	, ,
distance	AB	11.4 ± 0.2	pc	van Leeuwen (2007)
$M_{ m bol}$	AB	7.90	mag	Morales et al. (2008)
X (0.5–2.0 keV)	AB	975.10^{-17}	W/m2	Schwope et al. (2000)
B	AB	11.206	mag	Perryman et al. (1997)
V	AB	9.52	mag	Hawley et al. (1997)
V	AB	9.758 ± 0.026	mag	Kharchenko et al. (2007)
	В	> 13.2	mag	Henry et al. (1999)
	AB	9.73	mag	Bessel (1990)
R	AB	$8.81 {\pm} 0.026$	mag	???
R	AB	8.75	mag	Bessel (1990)
I	AB	7.67	mag	Bessel (1990)
J	AB	6.437 ± 0.021	mag	Cutri et al. (2003)
H	AB	5.786 ± 0.017	mag	Cutri et al. (2003)
$H (1.62 \mu \text{m})$	AB	5.75	mag	Morel & Magnenat (1978)
K	AB	5.578 ± 0.016	mag	Cutri et al. (2003)
	В	9.99	mag	Beuzit et al. (2004)
$L~(3.5\mu\mathrm{m})$	AB	5.40	mag	Morel & Magnenat (1978)
Variability	AB	V = 0.05	mag	Pojmanski et al. (2005)
		Hp = 0.11	mag	Pojmanski et al. (2005)
TiO5	AB	0.700	Å	Hawley et al. (1997); Morales et al. (2008)
$H\alpha EW$	AB	1.660	Å	Hawley et al. (1997); Morales et al. (2008)
		1.4 – 2.1	Å	Short & Doyle (1998)
$\log g$	AB	5.00		Alonso et al. (1996)
[Fe/H]	AB	0.00		Alonso et al. (1996)
$T_{ m eff}$	AB	3870	K	Alonso et al. (1996)
$v.\sin i$	AB	10	km/s	Short & Doyle (1998)
Rad.vel.	AB	-11.23 ± 0.11	$\rm km/s$	Nidever et al. (2002)
U	AB	-29.74 ± 1.00	$\rm km/s$	Montes et al. (2001)
V	AB	-18.54 ± 1.03	$\mathrm{km/s}$	Montes et al. (2001)
W	AB	-8.85 ± 4.83	$\mathrm{km/s}$	Montes et al. (2001)
Period		14.5	years	Heintz (1994)
Separation		5	A.U.	Beuzit et al. (2004)

$$M_J = 15.08 - 0.515 \times n + 0.0871 \times n^2 \text{ mag}$$
 (1)

$$M_H = 14.03 - 0.253 \times n + 0.0738 \times n^2 \text{ mag}$$
 (2)

$$M_K = 13.56 - 0.138 \times n + 0.0676 \times n^2 \text{ mag}$$
 (3)

where n is now the T spectral sub-type (e.g. n=0 for T0). It is clear that this function is not based on even the simplest modeling of the brown dwarf structure. The reduced χ^2 s are 56, 35 and 32 in the J, H and K bands respectively (the photometry is less accurate for the longer wavelengths), and the dispersions are 0.41 mag, 0.50 mag and 0.66 mag respectively. (In addition, the data are heterogeneous, with errors on the absolute magnitude ranging for 3–4% to 15–20%.) A proper relation between absolute magnitude and spectral type would take into account additional parameters, especially age. We use those relationships below to derive (rough) photometric distances of our isolated targets.

Ross 348C's absolute photometry would favour a T8 (J band) or even T7.5 (K band) spectral type.

With a similar spectral type (T8.5) and metallicity ([Fe/H] = -0.06 ± 0.20), the much redder J-K colour of Ross 458C compared to that of Wolf 940B is a clear indication of its lower gravity, which produces a reduced H₂ collision-induced absorption in the K band.

The z-J, J-H and H-K colours of Ross 458C are also within 1σ of those of ULAS J003402.77–005206.7, while Ross 348C is 0.3 mag redder in Y-J than ULAS J0034 (but it is only a 3σ effect). The recent parallax of ULAS J0034 by Smart et al. (2009) gives a distance modulus of 0.21 \pm 0.11 mag larger than that of Ross 458C, so that the latter is 1.25 ± 0.12 mag brighter in absolute magnitude than ULAS J0034. Binarity (with a nearly equal-mass companion), a slightly earlier spectral type (e.g. T8.5, still compatible with identical colours), and/or a significantly larger distance to ULAS J0034 (e.g. 17 pc, at 1σ) could explain the discrepancy.

Alternatively, it could be due to the difference in age and mass (and radius). Leggett et al. (2009) has used

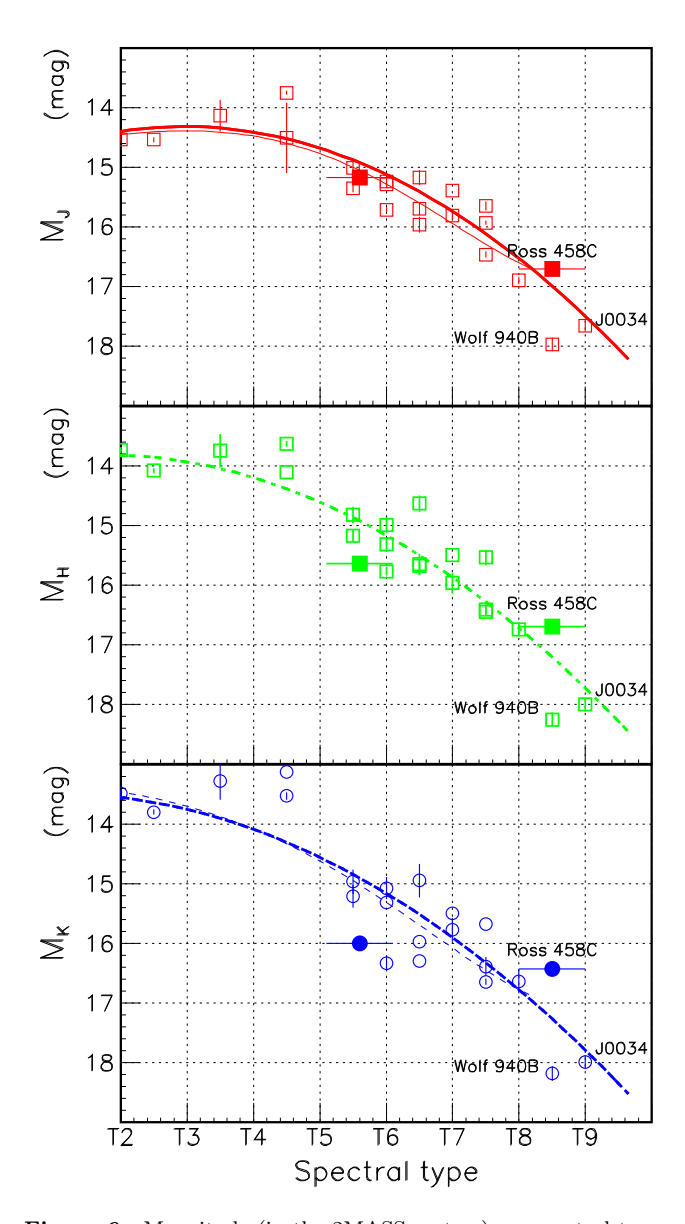


Figure 6. Magnitude (in the 2MASS system) vs. spectral type diagram for dwarfs later than T2, excluding known close binaries. We correct the UKIDSS magnitudes into the 2MASS system (see Appendix B). We overplot a tentative $2^{\rm nd}$ polynomial fit to the data, as well as the previous determination by Looper et al. (2008) in J and K, as thin lines.

Spitzer IRS 7.6–14.5 μ m spectroscopy, IRAC photometry as well as near-infrared spectroscopy and detailed modeling of ULAS J0034 to better constraints its parameters. They find a degeneracy between (higher) metallicity and (lower) gravity on the 2.2 and 4.5 μ m fluxes, but for the Solar metallicity of Ross 458AB and a distance of 16 pc, they favour $T_{\rm eff}=600\,{\rm K},~g=100\,{\rm m.s^{-2}},~R=0.12\,{\rm R}_{\odot},~M=5–8\,{\rm M_{Jup}}$ and an age of 0.1–0.2 Gyr. This is again a strong indication of the youth of Ross 458ABC, and the very small mass of Ross 458C

The spectral type we derive from the methane colour is extrapolated for spectral types later than T7, so the T8.9 \pm 0.3 classification we obtain for Ross 458C may have to be corrected. We use atmospheric models by Saumon & Marley

(2008) to calculate synthetic methane colour as a function of effective temperatures, for various gravities, to lower effective temperatures than those of our reference brown dwarfs. We plot the results in Fig.7.

We report the effective temperatures and methane colours for our known brown dwarfs, using the relation (6) of Stephens et al. (2009). We note that the effective temperatures of our mid- and late-T dwarfs seem offset compared to the models by $\sim 100\,\mathrm{K}$. The offset is even larger for the mid-T dwarfs when using the relationship of Golimowski et al. (2004). The methane line lists are known to be incomplete, which may explain the discrepancy for the mid-T dwarfs. For instance, the methane colour derived from the best model fit of SDSS J111009.99+011613.0, a red T5.5 dwarf, by Stephens et al. (2009) is bluer than what the observed spectrum indicates.

Liu et al. (2007) reports effective temperatures for two T7.5 of $\sim 800\,\mathrm{K}$, i.e. $100\,\mathrm{K}$ cooler than what Golimowski et al. (2004) or Stephens et al. (2009) predict for the T7 SDSS J162838.77+230821.1. On the other hand, Del Burgo et al. (2009), comparing high resolution spectroscopy with models, derive for four T7–T8 dwarfs temperatures systematically larger than 800– $900\,\mathrm{K}$ (1 σ).

We therefore do not attempt to derive an effective temperature for our targets based on their methane colours. Instead, we use the model colours in Fig. 7 to first conclude on the rather low dependency of the methane colour to the gravity: from 0 mag at $1000 \mbox{K}$ to $0.3 \mbox{ mag}$ at $500 \mbox{ K}$, over $1.3 \mbox{ orders}$ of gravity. This dependency is larger than our photometric errors for Ross $458 \mbox{C}$, but would not affect the effective temperature determination by more than $50 \mbox{ K}$ for any object cooler than $1100 \mbox{ K}$.

Secondly we can use the synthetic photometry to consistently estimate the range of mass and gravity based on the evolutionary models of Saumon & Marley (2008). For a model effective temperature of 500 K, and an age between 0.1 and 1 Gyr, their Fig.4 predicts for Ross 458C a gravity of 50 to $300\,\mathrm{m.s}^{-2}$, and a mass between 5 and 14 Jupiter masses.

4.1.3 Binding energy

From the spectral type of Ross 458A, we derive a mass of $0.6\,\mathrm{M}_\odot$ (Leggett 1992). The contribution of Ross 458B and C to the total mass of the system is negligible. At the current projected separation of $r\sin i = 1168\,\mathrm{A.U.}$, corresponding to 102'', the binding energy is:

$$E = 4.0.10^{42} \times \sin i \times \frac{m_{\text{Ross458C}}}{0.02 \text{M}_{\odot}} \text{erg}$$
 (4)

where i is the orbit inclination with respect to the line of sight.

In Fig.8 we reproduce the distribution of binary separation vs. total mass as compiled by Artigau et al. (2007), with Ross 458ABC. This system has a large separation compared to the main locus of binaries. Faherty et al. (2010) compiled a more complete list of wide binaries and discuss the distribution of binding energies. There are a dozen systems with a similar total mass and smaller binding energies. These authors also discuss the more frequent high-order multiplicity in weakly bound systems, which would help them survive disruption compared to simple binaries. In fact, Ross 458 is

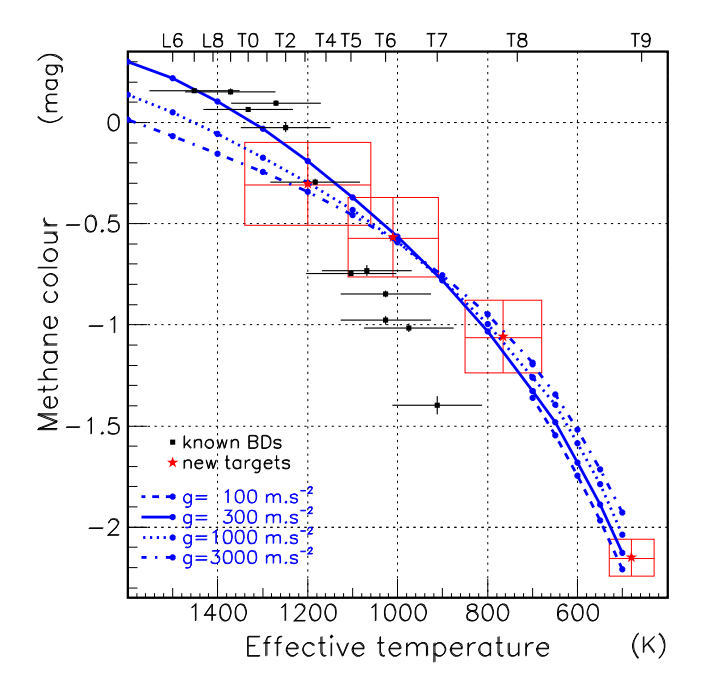


Figure 7. Methane colour for our new objects (stars, with error boxes), and synthetic photometry using the "no clouds" atmospheric models of Saumon & Marley (2008), for various gravities. We calculate the effective temperature of the reference brown dwarfs using the effective temperature vs. spectral type relationship of Stephens et al. (2009), which has a residual dispersion of $\approx 100 \, \mathrm{K}$ (squares, with error bars).

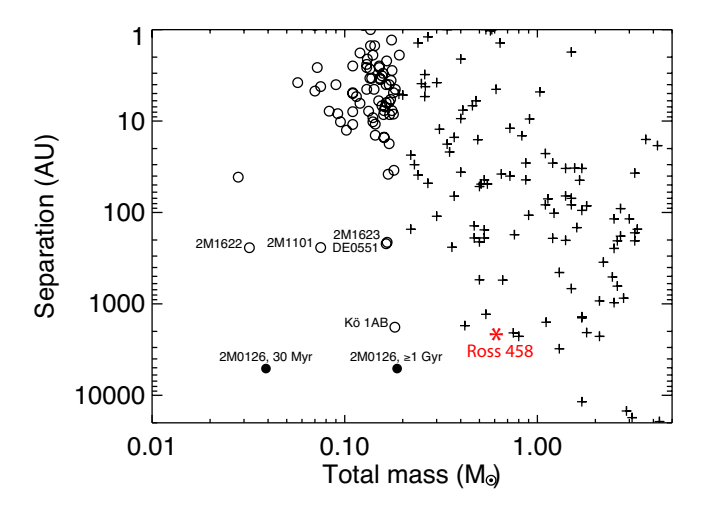


Figure 8. Separation of binaries as a function of total mass, from Artigau et al. (2007). The star represents Ross 458ABC.

a triple system, and the overluminosity of Ross 458C could be an indication of binarity.

4.2 Other targets

4.2.1 ULAS J1149-0143

ULAS J1149-0143 has a significant methane colour of 0.57 \pm 0.20. It is not detected in SDSS and must be a cool object. Its methane colour is more that 3σ away from those of M and L dwarfs. We estimate a spectral type of T5 \pm 1.5.

With a one-year baseline, we cannot measure the proper motion of ULAS J1149–0143, but place an upper-limit of $\sim 0.3''/{\rm yr}$, compatible with a distance as small as 20 pc and a tangential velocity as large as $30\,{\rm km/s}$. The photometric distance of a T5 dwarf with ULAS J1149–0143's J and K magnitudes would be $\sim 50\,{\rm pc}$.

4.2.2 ULAS J1153-0147

ULAS J1153-0147 has a significant methane colour of 1.06 ± 0.18 , 6σ away from those of M and L dwarfs. It is not detected in SDSS. We estimate a spectral type of T6.5 \pm 1.

measure the (large) proper motion ULAS J1153-0147 at 7σ . It is also the latest and the brightest of our targets after Ross 458C. It has a photometric distance of $\sim 29\,\mathrm{pc}$, and a tangential velocity of $\sim 85\,\mathrm{km/s}$. We ran a Besançon simulation of the field to estimate what fraction of stars with kinematics similar to ULAS J1153-0147. It has a velocity along V of $-50 \,\mathrm{km/s}$ to $-82 \,\mathrm{km/s}$ for a radial velocity between $-20 \,\mathrm{km/s}$ and $+30\,\mathrm{km/s}$ (66% of all stars have their radial velocity in this range). The model predicts that 60% of stars with such Vvelocities belong to the thick disk (this fraction decreases to 46% for a radial velocity range corresponding to 90% of stars in the field). The age dispersion of T-type dwarfs in the Solar neighbourhood is expected to differ from that of field stars (Allen et al. 2005), and therefore their velocity distributions may differ as well, but this gives an indication that ULAS J1153-0147 may be an old object.

There are no objects with a similar proper motion in our data, and none within 30 arcmin in Simbad.

4.2.3 ULAS J1303+1346

ULAS J1303+1346 has the weakest methane colour of our four targets. Taken at face value, it is only 2σ away from the stellar population, and therefore has a $\sim 2.5\%$ chance not to be a T dwarf. However, among the ~ 387 field stars, only six have a larger methane colour (1.6%), all detected in SDSS riz bands. (Among those six two are classified as galaxies by SDSS, two have ugr colours typical of quasars, and the last two are classified as stars.) Therefore, the probability for a given object to have a spurious (i.e. without methane absorption) methane colour of $-0.4\,\mathrm{mag}$ in this data set is < 2.5%. In addition, we selected the target because of its very red Y-J and blue J-H colours, hardly compatible with a stellar or a low-redshift quasar colour, and its UKIDSS stellar profile, incompatible for most galaxies of that brightness. Hence most contaminants are excluded. This does not prove its sub-stellar nature beyond any doubt, but it is very likely. With a one-year baseline, we fail to detect the proper motion of ULAS J1303+1346, but as for ULAS J1149-0143 this does not exclude that it is a brown dwarf.

5 CONCLUSIONS

We have searched $\approx 186 \, \text{sq.deg.}$ of UKIDSS Large Area Survey newly released in DR5+. Using simple colour and quality selection criteria, we selected four candidates for fast photometric follow-up with GROND on the ESO/MPG 2.2m

and Omega 2000 on the Calar Alto 3.5-m telescope. We present a calibration of the Omega 2000 methane filter set. Methane imaging confirms three T dwarfs and strongly supports the brown dwarf hypothesis of the fourth target. The latest-type target, Ross 458C, a T8-9 brown dwarf, is a companion to a M0.5+M6 binary which provides us with an accurate distance measurement (11.4 pc) and a rough age estimate (less than 1 Gyr). The absolute magnitudes and J-K colour point to a very young age, or possible binarity. Evolutionary models indicate a mass close to the deuterium burning minimum mass. This object will become an important well-characterised example of the latest T dwarfs. In addition we identify by proper motion and photometric distances two thick disk candidates, ULAS J1153-0147 and SDSS J1540+3742 (section A5).

ACKNOWLEDGMENTS

We thank Calar Alto Observatory for allocation of director's discretionary time to this programme and the observatory staff for its expeditious observations. We also thank Sascha Quanz for his precious comments, Steve Boudreault, Mark Marley, Annie Robin, and Markus Schmalz for their advice, and the referee Ben Burningham for his suggestions and corrections and his quick revision.

Part of the funding for GROND (both hardware as well as personnel) was generously granted from the Leibniz-Prize to Prof. G. Hasinger (DFG grant HA 1850/28–1).

This research has made use of the SIMBAD database, operated at C.D.S., Strasbourg, France, and of the M, L, and T dwarf compendium housed at <code>DwarfArchives.org</code> and maintained by C. Gelino, D. Kirkpatrick, and A. Burgasser.

The UKIDSS project is defined in Lawrence et al. (2007). UKIDSS uses the UKIRT Wide Field Camera (WF-CAM; Casali et al. 2007). The photometric system is described in Hewett et al. (2006), and the calibration is described in Hodgkin et al. (2009). The pipeline processing and science archive are described in Hambly et al. (2008). We thank the WSA support team for their help.

Funding for the SDSS and SDSS-II has been provided by the Alfred P. Sloan Foundation, the Participating Institutions, the National Science Foundation, the U.S. Department of Energy, the National Aeronautics and Space Administration, the Japanese Monbukagakusho, the Max Planck Society, and the Higher Education Funding Council for England. The SDSS Web Site is http://www.sdss.org/.

This publication makes use of data products from the Two Micron All Sky Survey, which is a joint project of the University of Massachusetts and the Infrared Processing and Analysis Center/California Institute of Technology, funded by the National Aeronautics and Space Administration and the National Science Foundation.

APPENDIX A: OMEGA2000 METHANE FILTER SET CALIBRATION

A1 Observations

To calibrate our methane filter set, in June 2008 we observed 12 reference brown dwarfs with known spectral type, derived

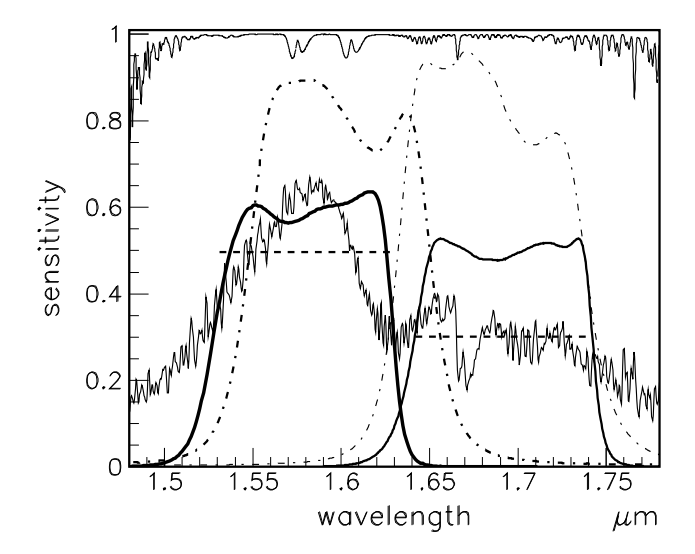


Figure A1. Complete filter sensitivity profile, including blocking filter and detector sensitivity (thick solid lines). The spectrum of the T5 2MASS J05591914-1404488 is overplotted (Cushing et al. 2005), its synthetic photometry (dashed lines), as well as the profiles of the AAT filters (only) used by Tinney et al. (2005), for comparison (dot-dashed lines), and a typical atmospheric transmission (solid line, top). Note that some measurements were provided by the manufacturer and corrected to the operating conditions.

from spectroscopy using the Burgasser et al. (2006) classification scheme. The spectral types vary from L7- to T7. We selected the targets (see Table A1 for their full names) based on their brightness, observability, and to obtain a good coverage of the late L and T spectral types. Here and through-out this article, we use the classification scheme of Burgasser et al. (2006) whenever available.

Observations were performed with the Omega 2000 instrument, mounted on the primary focus of the 3.5-m telescope at the Calar Alto Observatory in Spain. The filter profiles, including a blocking filter and the Omega2000 Hawaii 2 detection sensitivity, are shown in Fig. A1. The filters are well separated and well positioned with respect to the methane absorption feature, although some water absorption affects the methane off filter. Dithered exposures of around one minute were taken in the two filters of interest, methane off and on, and also in the H band. Exposures varied in number, due to observational constraints, but are always more numerous for the methane on filter, taking into account the lower expected flux in this band. Atmospheric conditions over the four nights of observation were good, with seeing varying from 0.9 to 1.2". Calibration frames such as dark exposures and dome or dusk flatfields were taken each night.

Preliminary treatment such as the construction of a bad-pixel map, flatfields for the two filters and a dark current image was performed using standard IRAF routines. Individual frame treatment, flatfielding, dark current- and bad pixel corrections as well as realignment and summation were carried out using the Omega 2000 data reduction pipeline, written by René Fassbender.

A first astrometry has been computed using koords¹ and the 2MASS catalog as reference. Photometric measurements were performed using SExtractor, over the large sample of the field stars and object. Since only relative photometry was of interest, no zero-point determination has been necessary. Depending on the extraction threshold, we observed wide dispersion for the faintest objects; hence we determined the zero-methane colour using a sample arbitrarily restricted to the 50 brightest objects. No distinction has been made between stars and galaxies for the determination of the zero-colour, as explained in section 2.3.

One of the targets, the T2.5 dwarf 2MASS J1546+4932, appeared closely blended to another star, because of its proper motion shift, and was rejected.

The results are presented in Table A1 and Fig. 4. We discuss the calibration of our photometry below in subsection A3.

A2 Synthetic photometry

To complement the observations described above we use the measured transmission profile of the methane filter set at 77 K, the operating temperature, to predict the synthetic colours of F to T7 dwarfs. We use the spectral libraries of IRTF/SpeX² (Cushing et al. 2005) and of Keck/NIRSPEC³ (McLean et al. 2003), which both provide calibrated F_{ν} spectra, with brown dwarfs as late as the T4.5 dwarf 2MASS J05591914–1404488 and the T8 2MASS J04151954–0935066 respectively.

We calculate the expected counts in each band and derive the methane colour in the AB system (we calculate the offset into the Vega system below). We find the methane colour to be insensitive to luminosity class (I–V) at the few mmag level.

A3 Photometric calibration

We present our colour measurements $H_{\rm off}-H_{\rm on}$ and the colours vs. spectral type relationships in the Vega system, with A0-type stars having a null colour.

A3.1 Synthetic photometry

Tinney et al. (2005) found a null colour for stars earlier than K. As the earliest dwarfs in Cushing et al. (2005) are F stars, we use the AB photometry of those to correct the synthetic AB photometry into the Vega system. We find an average AB colour of (-0.202 ± 0.003) mag with a dispersion of 1.1%.

The results are superimposed in Fig. 4. We fit a fourthorder polynomial function on both datasets independently:

$$C_m = (-16411 + 1106n - 4.67n^2 - 9.33n^3 - 1.211n^4).10^{-5}(A1)$$

$$C_m = (1783 + 43.0n - 21.26n^2 + 5.361n^3 - 0.4126n^4).10^{-4} (A2)$$

where n is the spectral type: n = -10 for M0, n = 0 for L0, n = 10 for T0, etc, for the IRTF/SpeX (valid for $n \leq 16$) and

www.atnf.csiro.au/computing/software/karma/

Keck/NIRSPEC, respectively. The dispersions are 29 mmag and 66 mmag respectively.

A3.2 Observations

In order to save telescope time under photometric conditions, we do not wish to observe spectro-photometric standard stars and perform a full calibration. Instead, we use the methane colours of the field stars, observed under the same seeing and transparency conditions, to correct the raw photometry into the Vega system. Stars have few absorption features in the H band, and Tinney et al. (2005) found that the methane colour in the AAT/IRIS2 system is a smooth, monotonic function of spectral type, and near-infrared colours, between the A and the early L spectral classes, with a peak-to-peak variation of less than $0.2\,\mathrm{mag}$.

Tinney et al. (2005) use their relationship between methane colour and near-infrared colours for A to M stars to derive the zero point. As we do not have observed methane colours for stars, we would have to rely on the synthetic photometry to perform the corrections. Instead, we estimate the mean colour of field objects and assign it a fix value.

Our sensitivity to stars with small methane colours is much larger in the $H_{\rm on}$ filter, because of the longer integration time in that filter. To avoid the Eddington bias which would lead to the overestimate of $H_{\rm off}$ fluxes of objects detected a low signal-to-noise ratios in the $H_{\rm off}$ band and large signal-to-noise ratios in the $H_{\rm on}$ band, we only consider bright enough sources.

The problem of the distinction between stars and galaxies arises, but we do not expect the latter to show any methane absorption feature. Emission-line galaxies may however show non-zero methane colours; galaxies of various types will also show a limited range of colours as B–M stars do. Possible aperture photometry biases due to the measurement of extended sources should not change from one filter to the next, but a different seeing between the two integrations may introduce systematics. As we limit ourselves to the brightest objects in the field, this eliminates most galaxies.

We run a Besançon model stellar simulation (Robin et al. 2003) of the field of Ross 458, whose stellar population, with a Galactic latitude of 75 deg, is typical of those of the UKIDSS–LAS fields. Combining the population simulation with the synthetic methane photometry of A–M stars, we obtain a mean methane AB colour of $-0.10\,\mathrm{mag}$ (corresponding to a K star), largely insensitive to the magnitude upper-limit.

The procedure is then to subtract from the target raw colour the mean raw colour of stars in the field, add $-0.10\,\mathrm{mag}$ to obtain the target AB colour, and subtract $-0.20\,\mathrm{mag}$ to derive the target Vega colour.

We fit a third-order polynomial function to the spectral type n (n = -10 for M0, n = 0 for L0, n = 10 for T0):

$$C_m = 0.273 - 0.0769 \times n + 0.0183 \times n^2 - 1.11.10^{-3} \times n^3$$
 (A3)

We ignore the photometric errors in the fit as some of them seem to be underestimated. The residual dispersion is 82 mmag.

Fig. 4 shows the good agreement between the predictions and the observations for T dwarfs later than T4. This gives us confidence that we can derive a precise spectral type

¹ Part of the Karma toolkit:

² http://irtfweb.ifa.hawaii.edu/~spex/IRTF_Spectral_Library/

³ http://www.astro.ucla.edu/~mclean/BDSSarchive/

Table A1. Calibration sample for the Omega 2000 methane filter set

Name	$H_{2\text{MASS}}$ Spectral Date ¹ type		Exp. time (min) Off On		Seeing (arcsec)	Methane colour	
SDSSp J134646.45-003150.4	15.46 ± 0.11	T6.5	Jun 20	6	15	1.1	-0.915 ± 0.033
2MASS J15031961+2525196	$13.86 {\pm} 0.03$	T5	Jun 20	6	15	1.1	-0.645 ± 0.013
SDSS J152039.82+354619.8	$14.58 {\pm} 0.05$	$T0\pm1$	Jun 20	6	9	1.1	$+0.165\pm0.011$
SDSS J152103.24+013142.7	$15.58 {\pm} 0.10$	T2	Jun 20	6	12	1.2	$+0.976\pm0.023$
2MASSI J1526140+204341	14.50 ± 0.04	$L7^2$	Jun 20	6	15	1.1	$+0.256\pm0.010$
SDSS J154009.36+374230.3	15.35 ± 0.10	$L9 \pm 1.5$	Jun 20	6	9	1.1	$+0.253\pm0.016$
2MASS J15461461+4932114	15.13 ± 0.09	$T2.5 \pm 1$	Jun 20	6	12	1.0	
2MASS J21392676+0220226	14.17 ± 0.05	T1.5	Jun 18-19	6	12	1.0	$+0.197\pm0.012$
2MASS J21543318+5942187	15.77 ± 0.17	T6	Jun 19-20	10	25	1.1	$-0.746 {\pm} 0.017$
SDSSp J162414.37+002915.6	15.52 ± 0.10	T6	Jun 21	10	25	0.9	-0.878 ± 0.021
SDSS J162838.77+230821.1	16.11 ± 0.15	T7	Jun 21	10	25	0.9	-1.297 ± 0.044
SDSS J163022.92+081822.0	16.33 ± 0.29	T5.5	Jun 18	10	25	1.1	-0.632 ± 0.027
SDSSp J175032.96+175903.9	$15.95 {\pm} 0.13$	T3.5	Jun 20	10	20	1.0	$-0.194{\pm}0.015$

¹ Year 2008. ² Optical classification (Kirkpatrick et al. 2000).

Table A2. Proper motion and astrometry of the calibration brown dwarfs, as well as the photometric distance and tangential velocity.

Name	MJD or Epoch	RA (J2000) hms	DEC (J2000) dms	μ_{α} (mas/yr)	μ_{δ} (mas/yr)	dist. pc	$v_{\perp} m km/s$
SDSSp J1346-0031	2004.706	13 46 46.252	-00 31 50.88	-505 ± 14	-105 ± 14	14.6^{1}	35
$2MASS\ J1503+2525$	2004.508	$15\ 03\ 19.641$	$+25\ 25\ 22.51$	$+75\pm12$	$+560\pm17$	7	19
SDSS J1520+3546	2003.312	$15\ 20\ 39.828$	$+35\ 46\ 19.84$	$+308\pm12$	-374 ± 13	13	27
SDSS J1521+0131	2007.552	$15\ 21\ 03.165$	$+01\ 31\ 43.11$	-219 ± 28	$+59\pm32$	24	26
2MASSI J1526+2043	2000.205	$15\ 26\ 14.005$	$+20\ 43\ 40.48$	-227 ± 12	-358 ± 13	6	12
SDSS J1540+3742	2004.339	$15\ 40\ 09.344$	$+37\ 42\ 29.99$	-226 ± 14	-382 ± 15	16^{2}	44
$2MASS\ J1546+4932$	2006.690	$15\ 46\ 14.829$	$+49\ 32\ 13.51$	-40 ± 34	$+731\pm17$	19	67
$2MASS\ J2139+0220$	2003.256	$21\ 39\ 26.858$	$+02\ 20\ 23.09$	$+490 \pm 15$	$+144 \pm 16$	13	31
2MASS J2154+5942	2007.254	$21\ 54\ 33.186$	$+59\ 42\ 19.00$	-1 ± 18	$+31\pm18$	13	2
SDSSp J1624+0029	2002.773	$16\ 24\ 14.275$	$+00\ 29\ 15.77$	-388 ± 11	$+0\pm11$	11^{3}	20
SDSS J1628+2308	2006.084	$16\ 28\ 38.854$	$+23\ 08\ 19.98$	$+418\pm21$	-438 ± 21	12	34
SDSS J1630+0818	2007.345	$16\ 30\ 22.909$	$+08\ 18\ 21.57$	-76 ± 38	-87 ± 37	18	10
SDSSp J1750+1759	2007.822	$17\ 50\ 33.048$	$+17\ 59\ 04.79$	$+183\pm33$	$+62 \pm 33$	27^{3}	24

¹ Tinney et al. (2003). ² Looper et al. (2008) give a photometric distance of 22 pc, within 2σ of our value. We use their estimate as our relationship does not apply for L dwarfs. ³ Vrba et al. (2004).

based on our methane colour. The agreement is not so good for ${\rm L/T}$ transition brown dwarfs.

A4 Systematic uncertainties

The errors on the spectral type derived from the methane colour are the sum of the photometric errors on the methane colour measurement for each target, and of systematic errors resulting from the photometric errors and spectral type errors of the reference brown dwarfs and the possibly inappropriate fitted function. We can use the dispersion around the fitted functions to estimate the systematic errors. The dispersion for the observed methane colours is larger than that derived from the synthetic photometry, so we conservatively use it hereafter. Because the slope of the relationship becomes steeper for later objects, the systematic error decreases with spectral type, from 0.29 subtype at T5 to 0.16 subtype at T8.

The dispersion, however, does not reproduce all the contributions to the systematic error, because our refer-

ence sample is small, and may not be representative, in terms of e.g. gravity or dust composition, of our target sample (we note however that both samples are magnitude-limited). From Fig. 7, we see however that the sensitivity of the method to the gravity is modest for spectral types later than T6, at about 0.2 subtype over a range of $g=100-3000\,\mathrm{m.s^{-2}}$, to 1 subtype at T4, and much more for earlier types. Because our reference sample includes objects of various gravities, this contribution is already partly taken into account in the fit dispersion, but we conservatively add it to the systematic errors.

A5 Proper motions and companions

We use the discovery positions and our Omega 2000 positions to derive the positions of all objects in the Omega 2000 field of view. We perform the image registration of the Omega 2000 data using the discovery catalogue as the astrometric reference, using the same technique as for the targets (see Section 2.2). The results are presented in Ta-

ble A2. We obtain a good agreement with published values, such as those of Tinney et al. (2003). However our values significantly differ from those of Jameson et al. (2008) for 2MASS J1503+2525 and SDSS J1521+0131.

All the transverse velocities we measure are typical of thin disk velocities, except those of 2MASS J1546+4932 and SDSS J1540+3742. The former has a positive velocity along the Galactic rotation direction V for a wide range of radial velocities, and therefore belong to the thin disk. As in section 4.2.2, a Besançon simulation of the field to estimate what fraction of stars with kinematics similar to the latter. SDSS J1540+3742 has a velocity along V of $-80 \,\mathrm{km/s}$ to $-43 \,\mathrm{km/s}$ for a radial velocity between $-50 \,\mathrm{km/s}$ and +20 km/s (63% of all stars have their radial velocity in this range). The model predicts that 63% of stars with such V velocities belong to the thick disk (this fraction decreases slightly for a larger range of radial velocities). It is therefore possibly a thick disk object, but it is not possible to assign it with certainty to the thick disk population based on our data.

We also searched for other T dwarfs in the field of view, using the methane colour. We found none, but we identified an object, SDSS J163023.89+081230.9, with a colour corresponding to a T5 dwarf, but with ugriz SDSS detections. Because of this and of its optical colours, it is most likely a $z\approx 1.4$ quasar, in a side area covered by SDSS but not by the SDSS QSO survey (Fan, priv. com.).

APPENDIX B: UKIDSS–2MASS COLOUR TRANSFORMATIONS

We have used the UKIDSS and 2MASS magnitudes calculated by Hewett et al. (2006) of 52 ultracool dwarfs (22 T dwarfs) to fit second-order polynomials of the UKIDSS–2MASS colours as a function of (infrared) spectral types (see Fig. B1). We obtain:

$$M_J = -0.136 - 0.0127 \times n - 0.00085 \times n^2 \text{ mag}$$
 (B1)

$$M_H = +0.058 - 0.0011 \times n - 0.00031 \times n^2 \text{ mag}$$
 (B2)

$$M_K = +0.017 + 0.0116 \times n + 0.00097 \times n^2 \text{ mag}$$
 (B3)

where n is the T spectral sub-type (e.g. n=0 for T0). The dispersions are 1.0%, 0.6% and 1.5% in the J, H and K band respectively.

We searched the UKIDSS DR6 Large Area Survey and Galactic Cluster Survey catalogues for UKIDSS magnitudes of ultracool dwarfs detected by 2MASS, within 5''. Unfortunately, 2MASS measurements of T-type dwarfs with good accuracy (< 0.2 mag) are scarce, especially at longer wavelengths. Removing the worst outlier and subtracting the 2MASS and UKIDSS photometric errors, we find a dispersion of 6%, 9% and 1% in the J, H and K bands respectively, based on 9, 14 and 8 objects.

Finally we compare our transformations with those that Stephens & Leggett (2004) obtained between the 2MASS and MKO systems (the WFCam filter set was designed to match the MKO system, Hewett et al. 2006). The agreement is excellent except in the J band, for which we measure $J_{\rm UKIDSS}-J_{\rm 2MASS}$ colours 3% (5%) larger for L- (T-, resp.) type dwarfs than the $J_{\rm MKO}-J_{\rm 2MASS}$ colours of Stephens & Leggett (2004).

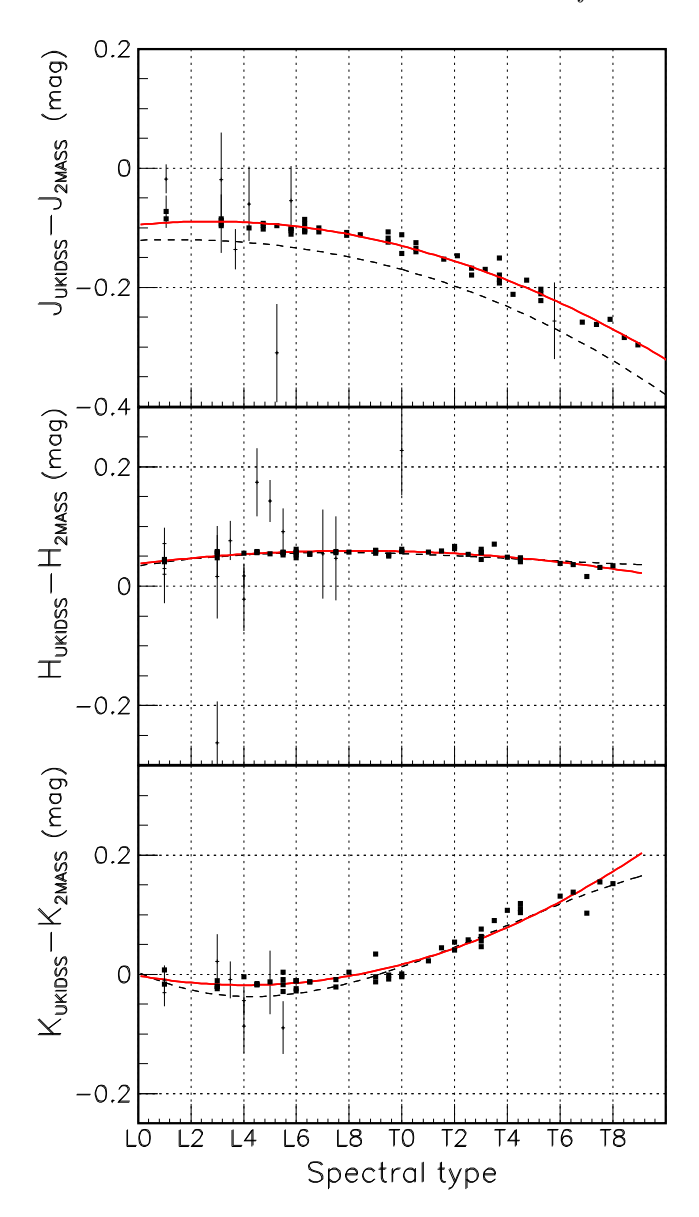


Figure B1. UKIDSS-2MASS colours as a function of spectral type, for 52 ultracool dwarfs (square, from Hewett et al. 2006), as red solid lines. We superimpose the observed colours of ultracool dwarfs with 2MASS detections, observed with UKIDSS (with error bars). We superimpose the transformations between the MKO and 2MASS systems of Stephens & Leggett (2004) as black dashed lines.

REFERENCES

Allard F., Hauschildt P. H., Alexander D. R., Tamanai A., Schweitzer A., 2001, ApJ, 556, 357

Allen P. R., Koerner D. W., Reid I. N., Trilling D. E., 2005, ApJ, 625, 385

Alonso A., Arribas S., Martinez-Roger C., 1996, A&AS, 117, 227

Artigau É., Lafrenière D., Doyon R., Albert L., Nadeau D., Robert J., 2007, ApJ, 659, L49

Bailer-Jones C. A., Bizenberger P., Storz C., 2000, in Iye M., Moorwood A. F., eds, Society of Photo-Optical Instrumentation Engineers (SPIE) Conference Series Vol. 4008, 2000, p. 1305

- Baraffe I., Chabrier G., Allard F., Hauschildt P. H., 1998, A&A, 337, 403
- Bertin E., 2006, in Gabriel C., Arviset C., Ponz D., Enrique S., eds, ASP Conf. Ser. 351, 2005, p.112
- Bertin E., Arnouts S., 1996, A&AS, 117, 393
- Bessel M. S., 1990, A&AS, 83, 357
- Beuzit J.-L., Ségransan D., Forveille T., Udry S., Delfosse X., Mayor M., Perrier C., Hainaut M.-C., Roddier C., Roddier F., Martín E. L., 2004, A&A, 425, 997
- Burgasser A. J., 2004, ApJ, 614, L73
- Burgasser A. J., Geballe T. R., Leggett S. K., Kirkpatrick J. D., Golimowski D. A., 2006, ApJ, 637, 1067
- Burningham B., Pinfield D. J., Leggett S. K., Tamura M., Lucas P. W., Homeier D., Day-Jones A., Jones H. R. A., Clarke J. R. A., Ishii M., Kuzuhara M., Lodieu N., Zapatero Osorio M. R., Venemans B. P., Mortlock D. J., Barrado Y Navascués D., Martin E. L., Magazzù A., 2008, MNRAS, 391, 320
- Burningham B., Pinfield D. J., Leggett S. K., Tinney C. G., Liu M. C., Homeier D., West A. A., Day-Jones A., Huelamo N., Dupuy T. J., Zhang Z., Murray D. N., Lodieu N., Barrado Y Navascués D., Folkes S., Galvez-Ortiz M. C., Jones H. R. A., Lucas P. W., Calderon M. M., Tamura M., 2009, MNRAS, 395, 1237
- Burrows A., Sudarsky D., Hubeny I., 2006, ApJ, 640, 1063 Burrows A., Sudarsky D., Lunine J. I., 2003, ApJ, 596, 587 Casali M., Adamson A., Alves de Oliveira C., Almaini O., Burch K., Chuter T., Elliot J., Folger M., Foucaud S., Hambly N., Hastie M., Henry D., Hirst P., Irwin M., Ives D., Lawrence A., Laidlaw K., Lee D., Lewis J., Lunney D., McLay S., Montgomery D., Pickup A., Read M., Rees N., Robson I., Sekiguchi K., Vick A., Warren S., Woodward B., 2007, A&A, 467, 777
- Chiu K., Liu M. C., Jiang L., Allers K. N., Stark D. P., Bunker A., Fan X., Glazebrook K., Dupuy T. J., 2008, MNRAS, 385, L53
- Cushing M. C., Rayner J. T., Vacca W. D., 2005, ApJ, 623, 1115
- Cutri R. M., Skrutskie M. F., van Dyk S., Beichman C. A., Carpenter J. M., Chester T., Cambresy L., Evans T., Fowler J., Gizis J., Howard E., Huchra J., Jarrett T., Kopan E. L., Kirkpatrick J. D., Light R. M., Marsh K. A., McCallon H., Schneider S., Stiening R., Sykes M., Weinberg M., Wheaton W. A., Wheelock S., Zacarias N., 2003, 2MASS All Sky Catalog of point sources.
- Del Burgo C., Martín E. L., Zapatero Osorio M. R., Hauschildt P. H., 2009, A&A, 501, 1059
- DeGennaro S., von Hippel T., Jefferys W. H., Stein N., van Dyk D., Jeffery E., 2009, ApJ, 696, 12
- Delfosse X., Tinney C. G., Forveille T., Epchtein N., Borsenberger J., Fouqué P., Kimeswenger S., Tiphène D., 1999, A&AS, 135, 41
- Delorme P., Delfosse X., Albert L., Artigau E., Forveille T., Reylé C., Allard F., Homeier D., Robin A. C., Willott C. J., Liu M. C., Dupuy T. J., 2008, A&A, 482, 961
- Ducourant C., Le Campion J. F., Rapaport M., Camargo J. I. B., Soubiran C., Périe J. P., Teixeira R., Daigne G., Triaud A., Réquième Y., Fresneau A., Colin J., 2006, A&A, 448, 1235
- Faherty J. K., Burgasser A. J., West A. A., Bochanski J. J., Cruz K. L., Shara M. M., Walter F. M., 2010, AJ, 139, 176

- Goldman B., Delfosse X., Forveille T., Afonso C., Alard C., Albert J. N., Andersen J., Ansari R., Aubourg É., Bareyre P., Bauer F., Beaulieu J. P., Borsenberger J., Bouquet A., Char S., Charlot X., Couchot F., Coutures C., Derue F., Ferlet R., Fouqué P., Glicenstein J. F., Gould A., Graff D., Gros M., Haissinski J., Hamilton J. C., Hardin D., de Kat J., Kim A., Lasserre T., Lesquoy É., Loup C., Magneville C., Mansoux B., Marquette J. B., Martín E. L., Maurice É., Milsztajn A., Moniez M., Palanque-Delabrouille N., Perdereau O., Prévot L., Regnault N., Rich J., Spiro M., Vidal-Madjar A., Vigroux L., Zylberajch S. t., 1999, A&A, 351, L5
- Golimowski D. A., Leggett S. K., Marley M. S., Fan X., Geballe T. R., Knapp G. R., Vrba F. J., Henden A. A., Luginbuhl C. B., Guetter H. H., Munn J. A., Canzian B., Zheng W., Tsvetanov Z. I., Chiu K., Glazebrook K., Hoversten E. A., Schneider D. P., Brinkmann J., 2004, AJ, 127, 3516
- Greiner J., Bornemann W., Clemens C., Deuter M., Hasinger G., Honsberg M., Huber H., Huber S., Krauss M., Krühler T., Küpcü Yoldaş A., Mayer-Hasselwander H., Mican B., Primak N., Schrey F., Steiner I., Szokoly G., Thöne C. C., Yoldaş A., Klose S., Laux U., Winkler J., 2008, PASP, 120, 405
- Greiner J., Bornemann W., Clemens C., Deuter M., Hasinger G., Honsberg M., Huber H., Huber S., Krauss M., Krühler T., Küpcü Yoldas A., Mayer-Hasselwander H., Mican B., Primak N., Schrey F., Steiner I., Szokoly G., Thöne C. C., Yoldas A., Klose S., Laux U., Winkler J., 2007, The Messenger, 130, 12
- Hambly N. C., Collins R. S., Cross N. J. G., Mann R. G.,
 Read M. A., Sutorius E. T. W., Bond I., Bryant J., Emerson J. P., Lawrence A., Rimoldini L., Stewart J. M.,
 Williams P. M., Adamson A., Hirst P., Dye S., Warren S. J., 2008, MNRAS, 384, 637
- Helling C., Ackerman A., Allard F., Dehn M., Hauschildt P., Homeier D., Lodders K., Marley M., Rietmeijer F., Tsuji T., Woitke P., 2008, MNRAS, 391, 1854
- Helling C., Dehn M., Woitke P., Hauschildt P. H., 2008, ApJ, 675, L105
- Henry T. J., Franz O. G., Wasserman L. H., Benedict G. F., Shelus P. J., Ianna P. A., Kirkpatrick J. D., McCarthy Jr. D. W., 1999, ApJ, 512, 864
- Hewett P. C., Warren S. J., Leggett S. K., Hodgkin S. T., 2006, MNRAS, 367, 454
- Hodgkin S. T., Irwin M. J., Hewett P. C., Warren S. J., 2009, MNRAS, 394, 675
- Jameson R. F., Casewell S. L., Bannister N. P., Lodieu N., Keresztes K., Dobbie P. D., Hodgkin S. T., 2008, MNRAS, 384, 1399
- Kharchenko N. V., Scholz R., Piskunov A. E., Roeser S., Schilbach E., 2007, VizieR Online Data Catalog, 3254, 0 Kirkpatrick J. D., Cruz K. L., Barman T. S., Burgasser A. J., Looper D. L., Tinney C. G., Gelino C. R., Lowrance P. J., Liebert J., Carpenter J. M., Hillenbrand L. A., Stauffer J. R., 2008, ApJ, 689, 1295
- Kirkpatrick J. D., Reid I. N., Liebert J., Gizis J. E., Burgasser A. J., Monet D. G., Dahn C. C., Nelson B., Williams R. J., 2000, AJ, 120, 447
- Lawrence A., Warren S. J., Almaini O., Edge A. C., Ham-

- bly N. C., Jameson R. F., Lucas P., Casali M., Adamson A., Dye S., Emerson J. P., Foucaud S., Hewett P., Hirst P., Hodgkin S. T., Irwin M. J., Lodieu N., McMahon R. G., Simpson C., Smail I., Mortlock D., Folger M., 2007, MN-RAS, 379, 1599
- Leggett S. K., 1992, ApJS, 82, 351
- Leggett S. K., Cushing M. C., Saumon D., Marley M. S., Roellig T. L., Warren S. J., Burningham B., Jones H. R. A., Kirkpatrick J. D., Lodieu N., Lucas P. W., Mainzer A. K., Martín E. L., McCaughrean M. J., Pinfield D. J., Sloan G. C., Smart R. L., Tamura M., Van Cleve J., 2009, ApJ, 695, 1517
- Leggett S. K., Geballe T. R., Fan X., Schneider D. P., Gunn J. E., Lupton R. H., Knapp G. R., Strauss M. A., McDaniel A., Golimowski D. A., Henry T. J., Peng E., Tsvetanov Z. I., Uomoto A., Zheng W., Hill G. J., Ramsey L. W., Anderson S. F., Annis J. A., Bahcall N. A., Brinkmann J., Chen B., Csabai I., Fukugita M., Hennessy G. S., Hindsley R. B., Ivezić Ž., Lamb D. Q., Munn J. A., Pier J. R., Schlegel D. J., Smith J. A., Stoughton C., Thakar A. R., York D. G., 2000, ApJ, 536, L35
- Leggett S. K., Hauschildt P. H., Allard F., Geballe T. R., Baron E., 2002, MNRAS, 332, 78
- Liu M. C., Leggett S. K., Chiu K., 2007, ApJ, 660, 1507
 Lodieu N., Pinfield D. J., Leggett S. K., Jameson R. F.,
 Mortlock D. J., Warren S. J., Burningham B., Lucas
 P. W., Chiu K., Liu M. C., Venemans B. P., McMahon
 R. G., Allard F., Baraffe I., Barrado y Navascués D., Carraro G., Casewell S. L., Chabrier G., Chappelle R. J.,
 Clarke F., Day-Jones A. C., Deacon N. R., Dobbie P. D.,
 Folkes S. L., Hambly N. C., Hewett P. C., Hodgkin S. T.,
 Jones H. R. A., Kendall T. R., Magazzù A., Martín E. L.,
 McCaughrean M. J., Nakajima T., Pavlenko Y., Tamura
 M., Tinney C. G., Zapatero Osorio M. R., 2007, MNRAS,
 379, 1423
- Lodieu N., Dobbie P. D., Deacon N. R., Venemans B. P., Durant M., 2009, MNRAS, 395, 1631
- Looper D. L., Gelino C. R., Burgasser A. J., Kirkpatrick J. D., 2008, ApJ, 685, 1183
- Luyten W. J., 1979, LHS catalogue. A catalogue of stars with proper motions exceeding 0"5 annually
- McLean I. S., McGovern M. R., Burgasser A. J., Kirkpatrick J. D., Prato L., Kim S. S., 2003, ApJ, 596, 561
- Montes D., López-Santiago J., Gálvez M. C., Fernández-Figueroa M. J., De Castro E., Cornide M., 2001, MNRAS, 328, 45
- Morales J. C., Ribas I., Jordi C., 2008, A&A, 478, 507 Morel M., Magnenat P., 1978, A&AS, 34, 477
- Nakajima T., Oppenheimer B. R., Kulkarni S. R., Golimowski D. A., Matthews K., Durrance S. T., 1995, Nature, 378, 463
- Nidever D. L., Marcy G. W., Butler R. P., Fischer D. A., Vogt S. S., 2002, ApJS, 141, 503
- Perryman M. A. C., Lindegren L., Kovalevsky J., Hoeg E., Bastian U., Bernacca P. L., Crézé M., Donati F., Grenon M., van Leeuwen F., van der Marel H., Mignard F., Murray C. A., Le Poole R. S., Schrijver H., Turon C., Arenou F., Froeschlé M., Petersen C. S., 1997, A&A, 323, L49
- Pinfield D. J., Burningham B., Tamura M., Leggett S. K., Lodieu N., Lucas P. W., Mortlock D. J., Warren S. J., Homeier D., Ishii M., Deacon N. R., McMahon R. G., Hewett P. C., Osori M. R. Z., Martin E. L., Jones H. R. A.,

- Venemans B. P., Day-Jones A. C., Dobbie P. D., Folkes S. L., Dye S., Allard F., Baraffe I., Barrado Y Navascués D., Casewell S. L., Chiu K., Chabrier G., Clarke F., Hodgkin S. T., Magazzù A., McCaughrean M. J., Nakajima T., Pavlenko Y., Tinney C. G., 2008, MNRAS, 390, 304
- Pinfield D. J., Jones H. R. A., Lucas P. W., Kendall T. R., Folkes S. L., Day-Jones A. C., Chappelle R. J., Steele I. A., 2006, MNRAS, 368, 1281
- Pojmanski G., Pilecki B., Szczygiel D., 2005, Acta Astronomica, 55, 275
- Robin A. C., Reylé C., Derrière S., Picaud S., 2003, A&A, 409, 523
- Roeser S., Schilbach E., Schwan H., Kharchenko N. V., Piskunov A. E., Scholz R.-D., 2008, VizieR Online Data Catalog, 1312, 0
- Ross F. E., 1926, AJ, 37, 53
- Salim S., Gould A., 2003, ApJ, 582, 1011
- Saumon D., Marley M. S., 2008, ApJ, 689, 1327
- Schwope A., Hasinger G., Lehmann I., Schwarz R., Brunner H., Neizvestny S., Ugryumov A., Balega Y., Trümper J., Voges W., 2000, Astronomische Nachrichten, 321, 1
- Short C. I., Doyle J. G., 1998, A&A, 336, 613
- Smart R. L., Jones H. R. A., Lattanzi M. G., Leggett S. K., Warren S. J., Adamson A. J., Burningham B., Casali M., Evans D. W., Irwin M. J., Pinfield D., 2009, ArXiv eprints, 0912.3163
- Stephens D. C., Leggett S. K., 2004, PASP, 116, 9
- Stephens D. C., Leggett S. K., Cushing M. C., Marley M. S., Saumon D., Geballe T. R., Golimowski D. A., Fan X., Noll K. S., 2009, ApJ, 702, 154
- Tinney C. G., Burgasser A. J., Kirkpatrick J. D., 2003, AJ, 126, 975
- Tinney C. G., Burgasser A. J., Kirkpatrick J. D., McElwain M. W., 2005, AJ, 130, 2326
- Tsuji T., 2005, ApJ, 621, 1033
- van Leeuwen F., 2007, A&A, 474, 653
- Vrba F. J., Henden A. A., Luginbuhl C. B., Guetter H. H.,
 Munn J. A., Canzian B., Burgasser A. J., Kirkpatrick
 J. D., Fan X., Geballe T. R., Golimowski D. A., Knapp
 G. R., Leggett S. K., Schneider D. P., Brinkmann J., 2004,
 AJ, 127, 2948
- Warren S. J., Mortlock D. J., Leggett S. K., Pinfield D. J., Homeier D., Dye S., Jameson R. F., Lodieu N., Lucas P. W., Adamson A. J., Allard F., Barrado Y Navascués D., Casali M., Chiu K., Hambly N. C., Hewett P. C., Hirst P., Irwin M. J., Lawrence A., Liu M. C., Martín E. L., Smart R. L., Valdivielso L., Venemans B. P., 2007, MNRAS, 381, 1400
- West A. A., Hawley S. L., Bochanski J. J., Covey K. R., Reid I. N., Dhital S., Hilton E. J., Masuda M., 2008, AJ, 135, 785
- West A. A., Walkowicz L. M., Hawley S. L., 2005, PASP, 117, 706
- Zacharias N., Urban S. E., Zacharias M. I., Wycoff G. L., Hall D. M., Germain M. E., Holdenried E. R., Winter L., 2003, VizieR Online Data Catalog, 1289, 0
- Zuckerman B., Song I., Bessell M. S., 2004, ApJ, 613, L65